

# Direct imaging with highly diluted apertures. I. Field of view limitations

O. Lardi  re<sup>1</sup>  , F. Martinache<sup>2</sup> & F. Patru<sup>3</sup>

<sup>1</sup>Coll  ge de France, Observatoire de Haute-Provence, Saint-Michel-l’Observatoire, F-04870, France

<sup>2</sup>Department of Astronomy, Cornell University, Ithaca, NY 14853, USA

<sup>3</sup>Observatoire de la C  te d’Azur, Dpt. Gemini, UMR CNRS 6203, avenue Copernic, Grasse, F-06130, France

Accepted 2006 November 30. Received 2006 November 21; in original form 2006 March 7

## ABSTRACT

Future optical interferometric instrumentation mainly relies on the availability of an efficient cophasing system: once available, what has so far postponed the relevance of direct imaging with an interferometer will vanish. This paper focuses on the actual limits of snapshot imaging, inherent to the use of a sparse aperture: the number of telescopes and the geometry of the array impose the maximum extent of the field of view and the complexity of the sources. A second limitation may arise from the beam combination scheme. Comparing already available solutions, we show that the so called hypertelescope mode (or densified pupil) is ideal. By adjusting the direct imaging field of view to the useful field of view offered by the array, the hypertelescope makes an optimal use of the collected photons. It optimizes signal to noise ratio, drastically improves the luminosity of images and makes the interferometer compatible with coronagraphy, without inducing any loss of useful field of view.

**Key words:** instrumentation: high angular resolution – instrumentation: interferometers – techniques: interferometric.

## 1 INTRODUCTION

Over the last three decades, important scientific results have been obtained from long-baseline optical and infrared stellar interferometers concerning the stars and their environment, and more recently extragalactic sources (Rottgering et al. 2004). These results have been obtained thanks to sophisticated observing techniques, such as fringe visibilities and closure phase measurements (Baldwin et al. 1986).

Current interferometers involve between 2 and 4 telescopes only. The study of very complex and/or faint sources therefore requires many observations and image reconstruction techniques like aperture synthesis. Future interferometers should involve a large number of apertures ( $> 10$ ) in coherence (ideally in phase), but fringe visibility measurement appears no more suitable for such rich arrays. Indeed, visibility and closure phase measurements require either a pair-wise combination on different detectors, or an all-to-one combination in a non-redundant configuration, in order to isolate the signal provided by each baseline. This is a constraint that is difficult to satisfy in practice with a large number of beams in wide band. Moreover these combination

schemes are generally not compatible with stellar coronagraphy, for which a direct image featuring a bright central interference peak is required (Labeyrie 1996). For all these reasons, direct imaging involving an all-to-one beam combiner seems to be an elegant and simpler way to exploit a well-populated optical or infrared array.

However, many questions remain concerning the actual performances of future large arrays devoted to direct imaging, such as the field of view (FOV), the dynamic-range and the sensitivity. These parameters are crucial because they will impose the top-level requirements for the concept of future large interferometers, according to the expected science cases. This paper aims at giving some answers about the FOV of interferometers.

Owing to emerging Extremely Large Telescope projects, future optical interferometric arrays should exhibit very long baselines, typically kilometric, in order to really offer a complementary observing approach in terms of angular resolution. In this context, we consider here only highly diluted arrays. The associated pupil filling rate, given by:

$$r = n_T \times \frac{d^2}{D^2} , \quad (1)$$

\* E-mail: olivier.lardi  re@oamp.fr (OL); frantz@astro.cornell.edu (FM); fabien.patru@obs-azur.fr (FP)

tends towards zero, with  $n_T$  the number of telescopes of the array,  $d$  the diameter of an elementary aperture and  $D$  the

diameter of the whole interferometer. With a well populated, diluted array, for which we are only interested in high spatial frequencies and not by those measured by one elementary aperture (which therefore excludes LBT kind interferometers (Hinz et al. 2004)), direct imaging has been proved feasible thanks to Labeyrie's pupil densification technique (Labeyrie 1996; Pedretti et al. 2000; Gillet et al. 2003).

In his paper, Labeyrie tells us that direct imaging at the focus of a diluted array is possible if one densifies the pupil, either by zooming each elementary aperture or by moving them closer to each other, with a significant gain in sensitivity. The only condition is to keep the geometry of the array intact.

*A priori*, as long as one does not mix the frequencies sampled by the interferometer, the remapping of the pupil proposed by Labeyrie neither adds nor removes any useful information. However, being always compared to the purely homothetic (Fizeau) combination scheme, the so-called hypertelescope is known to provide direct imaging indeed, but on a limited FOV only. The notion of FOV for an interferometer is somewhat delicate, and actually requires the introduction of four different FOV. This distinction is essential to demonstrate that, the hypertelescope is an optimal optical image reconstruction technique inducing no useful FOV loss at all.

Section 2 highlights the influence of the array geometry on the FOV. Section 3 presents beam combination schemes already available for direct imaging whose FOV properties are compared in section 4 and discussed in section 5.

## 2 INFLUENCE OF THE ARRAY CONFIGURATION ON THE FOV

### 2.1 Number of apertures

Most current optical interferometers involve less than 4 telescopes working simultaneously. The observables, *i.e.* visibilities and closure quantities, are used in an inverse approach to constrain a model of the observed source: uniform or limb-darkened disk, binary system, etc. They are rarely sufficient to reconstruct a map or an image of the source, unlike what is achieved in radio interferometry (a recent example: Gitti et al. (2006)) and with aperture masking (Tuthill et al. 1999). Little therefore has been written about the limits of wide field imaging capabilities of an optical interferometer.

An interesting approach by Koechlin (2003) and Koechlin & Perez (2003) uses Shannon's theory of information to give a limit to the field-resolution ratio. The maximal amount of information that an interferometer can provide is proportional to the square root of the number of unique baselines in the array. In case of an extended filled source, this information amount can be converted in field-resolution ratio. For a non-redundant interferometer, this ratio is (Koechlin 2003):

$$\text{FOV}/\text{resolution} \leq \sqrt{n_T \times (n_T - 1)}, \quad (2)$$

with  $n_T$  the number of apertures in the array. This relation gives an upper limit to the usable FOV. We shall call this limit Information Field (IF). The IF only depends on the

number of apertures and the geometry of the array and not on the choice of a beam combiner scheme.

One can now reformulate the IF limitation another way. Because of the finite number of sub-apertures, which only offers a partial coverage of the spatial frequencies plane, an interferometer cannot provide the image of an arbitrarily complex extended source: this is known as the *crowding limit*. Let us decompose an extended source as a sum made of  $p$  elementary (*i.e.* non-resolved) sources. A point-like source seen by the interferometer can give a central peak surrounded by a halo or just a halo (Fig. 6).

The intensity of each central peak, resulting from the sum of  $n_T$  coherent contributions, is proportional to  $n_T^2$ . The average intensity of the halo however, is proportional to  $n_T$ , like its RMS fluctuation. After adding-up  $p$  elementary point-like sources, the resulting RMS fluctuation of the halo is now proportional to  $\sqrt{p} \times n_T$ .

Yet, a peak remains detectable by (incoherent) subtraction of the halo if it dominates the fluctuation of this halo. With  $SNR$  representing the signal-to-noise ratio that one desires the detection to have, this condition can be written as  $n_T^2 \geq SNR \times \sqrt{p} \times n_T$ , which imposes the crowding limit:

$$p \leq n_T^2 / SNR^2, \quad (3)$$

meaning that the number of observed sources must be less than the square of the number of apertures (Fig. 1). This crowding limit is of course at one with the field limit that was highlighted earlier: an image made of  $n_T \times n_T$  resels (resolution elements) cannot obviously provide information on more than  $n_T^2$  elementary sources. The IF can therefore be redefined as the maximal angular diameter of an extended filled source that can be directly imaged with  $SNR = 1$ .

### 2.2 Geometry of the array

The number of sub-apertures imposes the ultimate limits of FOV and crowding. Yet, the geometry of the array imposes the practical limits: the number of unique baselines and the PSF quality.

As with any classical telescope, the PSF of an interferometer is given by the Power Spectrum of the wavefront complex amplitude in the output pupil plane (Goodman 1996). For  $n_T$  identical sub-apertures of diameter  $d$  and position vector  $\rho_i$ , the PSF is given by:

$$I(\alpha) = A(\alpha) \times \left| \sum_{i=1}^{n_T} \exp \frac{-2i\pi \alpha \cdot \rho_i}{\lambda} \right|^2, \quad (4)$$

with  $\alpha$  the position vector in the image plane. Equation 4 reminds that this PSF is nothing but the product of two terms: an interference function, given by the exponential sum that is determined by the (eventually remapped) geometry of the array and an envelope  $A$ , whose shape and position depend on the retained beam combiner (Sec. 3).

For a well-populated array of maximum baseline  $D$ , the interference function is very similar to the diffraction pattern of a fully-filled aperture of diameter  $D$  (central peak and Airy rings), surrounded by a halo of sidelobes (speckles or high-order dispersed peaks) due to the holes of the pupil plane. According to the sampling theorem, the angular radius of the clean central part of the PSF is defined by  $\lambda/s$ ,

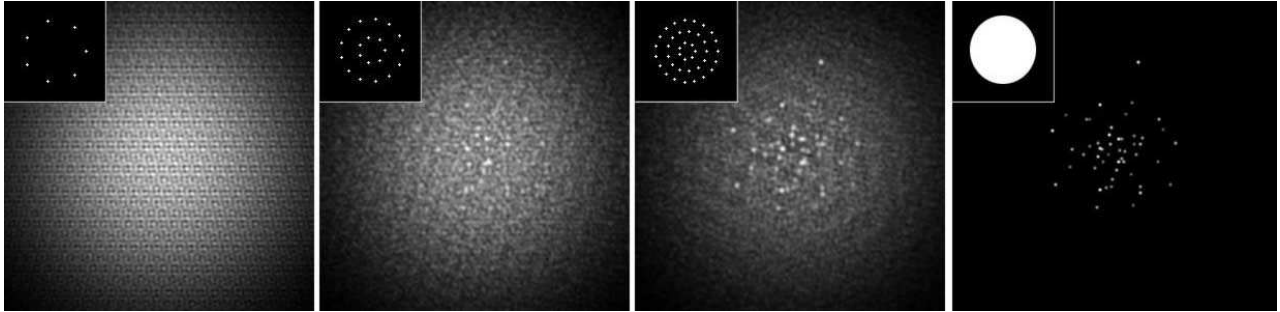


**Figure 1.** Direct images of a 50-stars cluster provided by a diluted interferometer involving 7, 20 and 39 apertures compared to a full-filled aperture (right). The crowding limit of each interferometer is respectively 5, 44 and 169 sources for  $SNR = 3$ . The 7-aperture case ( $1^{st}$  image) is well over the limit, but the 20-aperture case ( $2^{nd}$  image), where only the brightest stars exceed the background, corresponds to the crowding limit.

with  $s$  the distance between two adjacent apertures. For a non-regular array pattern, the clean part exhibits smoother edges, but we assume that  $\lambda/s$  still gives a good estimate of its mean radius, with  $s$  the “typical” smallest baseline in the array.

Consequently, two point-like sources can be observed properly and simultaneously only if their angular separation is lower than  $\lambda/s$ . Then, we can introduce the notion of a clean FOV (CLF) whose extent is simply:

$$CLF = \lambda/s. \quad (5)$$

One can demonstrate that the CLF is always smaller than the IF, whatever the array configuration. Indeed, expressed in units of  $\lambda/D$ , the diameter of the CLF and of the IF are respectively  $D/s$  and  $n_T$ . Then the condition  $CLF \leq IF$  implies  $D \leq n_T \times s$ , which is always true for a 2-dimensional array (there is equality for a linear regular array). A CLF smaller than the IF means that the crowding limit is not an issue, provided that one observes a source smaller than the CLF.

To illustrate the notion of CLF, figure 2 compares the interference function (*i.e.* the PSF without the envelope) of four different array configurations involving 39 apertures diluted over the same maximum baseline. These configurations actually correspond, with more or less fidelity to current proposals for future large interferometric arrays, whose names will therefore be used for convenience:

- **ELSA** (Quirrenbach 2004) is made of 13 regularly spaced telescopes along the 3 identical arms of a Y-configuration. ELSA can, to some extent, be considered as an anti-spider structure that traditionally bears the secondary mirror of telescopes.
- **OVLA** (Labeyrie, Koechlin, & Lemaître 1986), whose 39 telescopes are arranged non redundantly along a circle, can be considered as a giant telescope with a very important central obscuration.
- **KEOPS** (Vakili et al. 2004a), whose telescopes are arranged non redundantly along three concentric rings of 9, 13 and 19 telescopes, may be compared to a non-obstructed aperture.
- **CARLINA** (Le Coroller et al. 2004). Even if the geometry of the array is not fixed yet, a completely redundant square grid is often considered. The configuration retained here only uses 37 telescopes to provide a well-balanced array, inside a circle.

A glance at figure 2 makes us identify two distinct sparse aperture families. On the one hand, we have the OVLA and ELSA arrays, which definitely give priority to a relatively dense and homogeneous coverage of the  $(u, v)$  plane. They exhibit an “in-line” geometry, with therefore little space between telescopes and a rather extended CLF, whose diameter increases in proportion to the number of telescopes. ELSA presents preferred axis along which there is redundancy, whereas OVLA’s  $(u, v)$  coverage can be described by a purely radial function. This, of course, results in differences in the interference function: a centro-symmetric clean field for OVLA and the appearance of diffraction spikes for ELSA. For a better comparison, interference function profiles are sketched at figure 3.

On the other hand, there are the KEOPS and CARLINA arrays for which the priority is to have a uniform coverage of the pupil plane itself. The distance separating telescopes is therefore naturally enlarged which induces a reduction of the CLF: its diameter now only increases in proportion to the square root of the number of telescopes.

From the strong reduction of the CLF in the case of uniform arrays such as KEOPS and CARLINA, one may be tempted to exclude those configurations for direct imaging. However, what is lost in field is gained in dynamic-range: KEOPS and CARLINA offer a narrower but darker CLF than ELSA and OVLA (Fig. 3).

People working in stellar coronagraphy know that a mandatory condition to reach very high dynamic-range is at least a telescope with no central obscuration, possibly optimized by a prolate spheroidal apodization (Soummer et al. 2002). In those conditions, far from being uniformly flat, the associated Modulation Transfer Function or MTF (*i.e.* the  $(u, v)$  plan) exhibits a somewhat “conic” shape. This requirement is no different for the geometry of a diluted interferometer if it is made for high contrast imaging: the coverage of the pupil plane has to be privileged at the expense of the coverage of the  $(u, v)$  plane (Fig. 2). This statement concurs with the conclusions of Aime & Soummer (2003) who find that the best parameter to evaluate the relevance of the geometry of a diluted array designed for exoplanet detection is the integral of the square modulus of its MTF.

The choice of the geometry of the array must therefore be motivated by the primary scientific goal of the interferometer. OVLA and ELSA are definitely made for imaging of wide fields (multiple or extended sources such as interacting

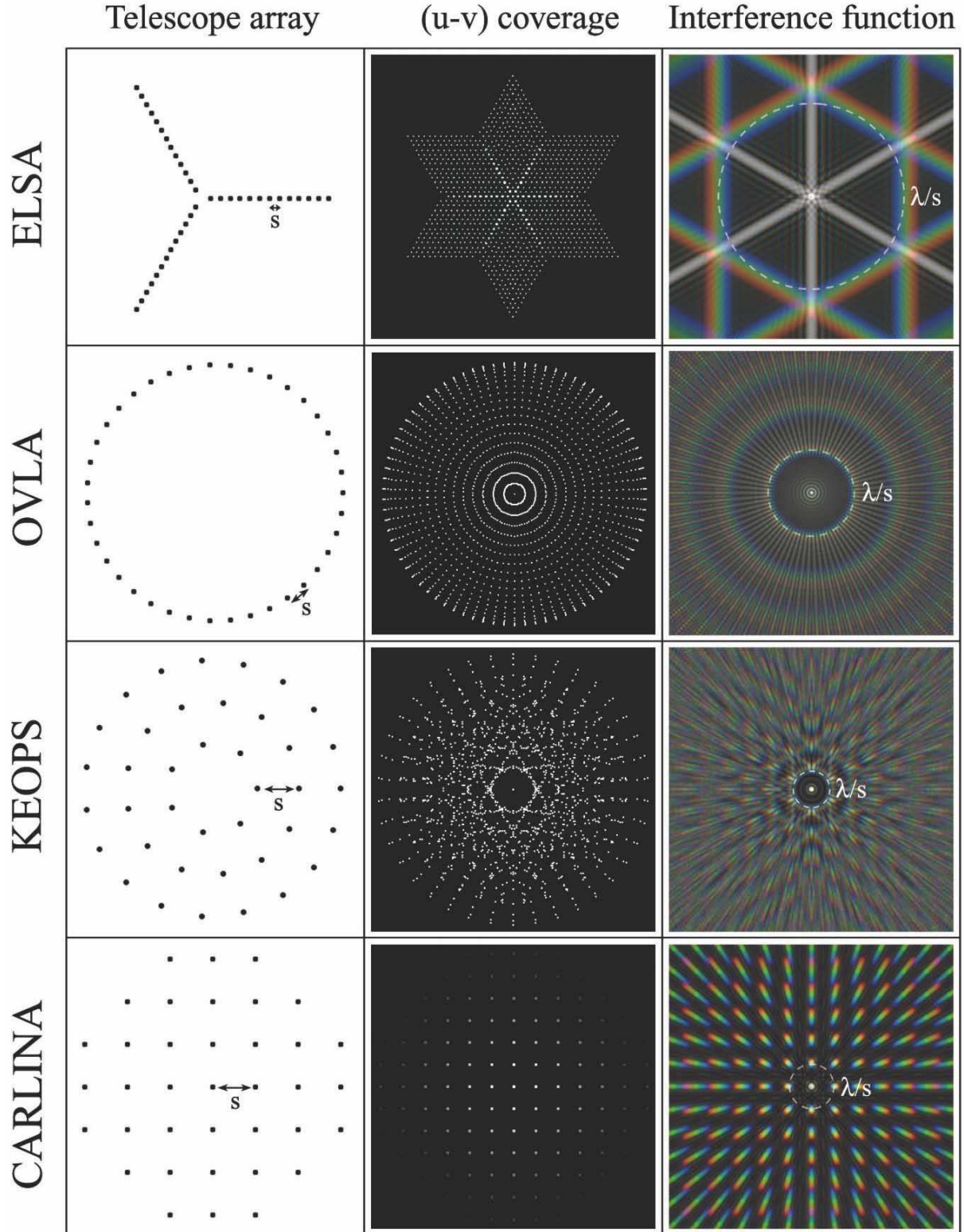


**Figure 2.** Telescope array configurations of four different interferometer proposals with their corresponding  $(u, v)$ -coverages (in grey levels) and their interference functions, *i.e.* PSF without envelope (polychromatic images with  $\Delta\lambda/\lambda = 0.2$ , intensity scale in power 0.3). For a fair comparison, these arrays all have the same maximum baseline and involve 39 telescopes (37 for CARLINA). The radius of the clean part of interference functions (*i.e.* the CLF size) is  $\lambda/s$ , with  $\lambda$  the central wavelength and  $s$  the typical minimum spacing between telescopes.

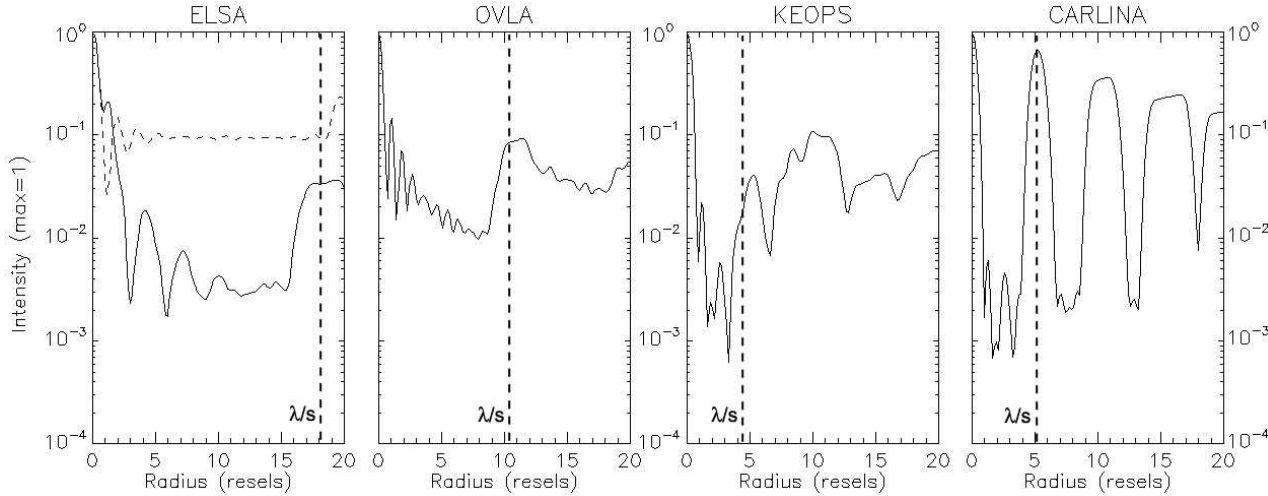


**Figure 3.** Radial profiles of the interference functions shown in figure 2 (maximum intensity normalized to 1, radius expressed in resels, with 1 resel =  $1.22 \lambda/D$ ). The best contrast of the image inside the Clean FOV ( $\lambda/s$ ) is from  $10^{-1}$  (in the vertical direction: dashed curve) to  $3 \cdot 10^{-3}$  (in the horizontal direction: solid curve) for ELSA,  $10^{-2}$  for OVLA,  $2 \cdot 10^{-3}$  for KEOPS, and  $8 \cdot 10^{-4}$  for CARLINA. Uniform arrays, as KEOPS and CARLINA, have a better dynamic-range, but a narrower CLF, than ELSA and OVLA.

binary stars, resolved stellar surfaces, envelopes and disks). KEOPS and CARLINA are better suited for high contrast imaging of compact sources and for exoplanet detection.

### 3 BEAM COMBINATION SCHEMES

This section focuses on the beam combination scheme, which determines the shape and the extent of the fringe envelope  $A$  (Equ. 4). The beam combiner can limit the FOV provided by the array if envelope  $A$  is narrower than the CLF. One has to introduce another FOV limitation, that does not depend on the geometry of the array but only on the beam combination scheme. This field is referred to as Direct Imaging FOV (DIF), *i.e.* the FOV inside which an image of a source can be formed directly. By definition, a point-like source is located inside the DIF if the central interference peak remains within envelope  $A$ .

Until now, three beam combination schemes have been considered for direct imaging: the Fizeau scheme, the Densified Pupil scheme (Labeyrie 1996), the IRAN scheme (Vakili et al. 2004b) and their fibred versions (Patru et al. 2006a). This section introduces a common formalism that describes these combiners and allows an homogeneous and quantitative comparison of their FOV properties.

#### 3.1 General formalism

To provide a directly exploitable image, a combiner may *a priori* perform a transformation of the wavefront at two different spatial frequency scales:

- a “high-frequency transformation”, which consists in displacing the sub-apertures centers, therefore altering the geometry of the array,
- a “low-frequency transformation”, which affects only the beams of each sub-aperture individually, such as a beam compression, a beam deflection, a pupil plane conjugation, a spatial filtering, etc.

The array is now reconfigured: let  $\rho_i$  and  $\rho'_i$  respectively represent the position vectors of the  $i^{th}$  aperture in the entrance and output pupil planes. Let also be  $\theta$ , the off-axis of the source, and  $\alpha$  the position vector in the image plane. Assuming that the interferometer is cophased on-axis (*i.e.* the optical paths of all arms are equal), the total optical path of the  $i^{th}$  beam is  $\theta \cdot \rho_i - \alpha \cdot \rho'_i$  (Fig. 4). Because of the additional term induced by the remapping, the PSF becomes non translation invariant: we have to update equation 4 that is now  $\theta$ -dependant:

$$I(\alpha, \theta) = A(\alpha) \times \left| \sum_{i=1}^{n_T} \exp \frac{-2i\pi \alpha \cdot \rho'_i}{\lambda} \cdot \exp \frac{2i\pi \theta \cdot \rho_i}{\lambda} \right|^2. \quad (6)$$

The first exponential term is the fringe pattern which depends only on the output pupil arrangement ( $\rho'_i$ ). The second exponential term contains the piston induced by the source off-axis  $\theta$ .

If the reconfiguration of the array is homothetic, we can introduce  $\gamma_b$ , so that  $\rho'_i = \gamma_b \rho_i$ . Equation 6 becomes:

$$I(\alpha, \theta) = A(\alpha) \times \left| \sum_{i=1}^{n_T} \exp \frac{-2i\pi(\alpha - \theta/\gamma_b) \cdot \rho'_i}{\lambda} \right|^2. \quad (7)$$

Now, if we denote as  $O(\theta)$  the object intensity distribution and

$$I_0(\alpha) = \left| \sum_{i=1}^{n_T} \exp \frac{-2i\pi \alpha \cdot \rho'_i}{\lambda} \right|^2 \quad (8)$$

the interference function, we can write, from equation 7, the intensity distribution for an extended source:

$$I(\alpha) = \iint O(\theta) A(\alpha) I_0(\alpha - \theta/\gamma_b) d^2\theta. \quad (9)$$

Assuming that envelope  $A$  is fixed and its extent is larger than the object size, one can take  $A$  out of the integral and approximate equation 9 as a convolution product

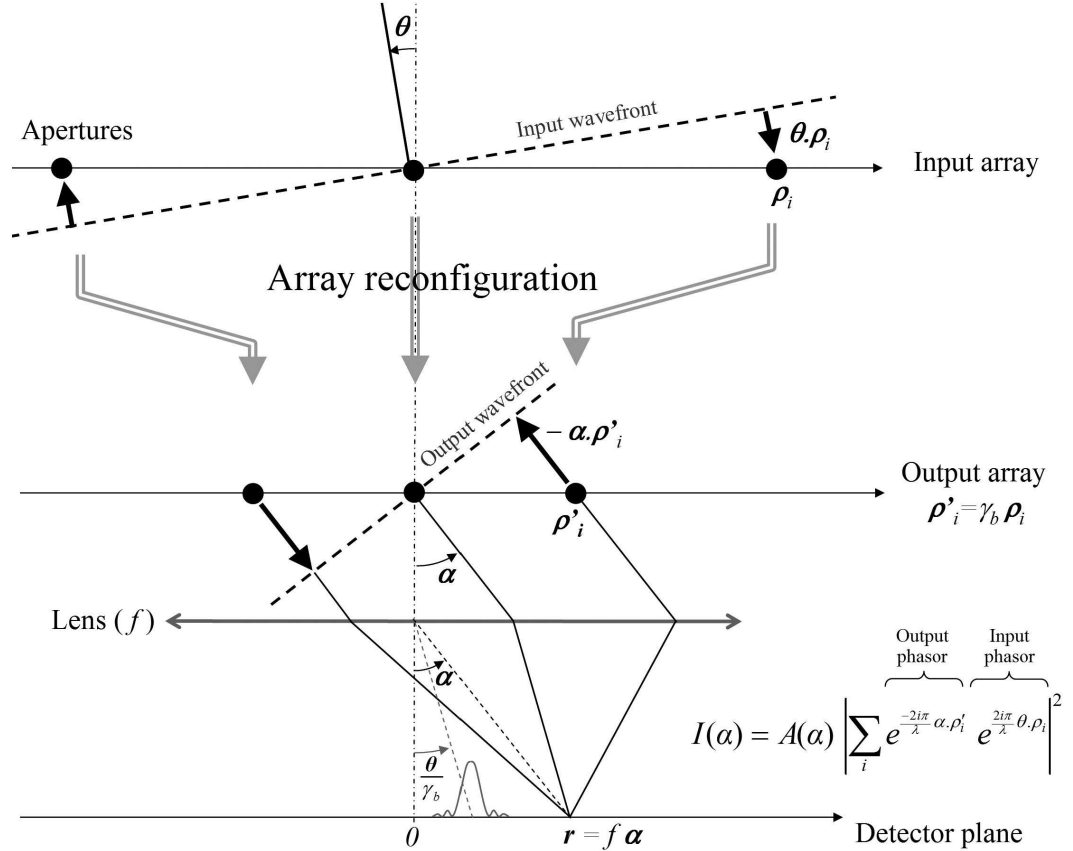


**Figure 4.** Optical path differences (OPD) induced by an array reconfiguration. Compared to the central beam ( $\rho = \rho' = 0$ ), the OPD cumulated by the  $i^{th}$  beam from the entrance sub-pupil (position  $\rho_i$ ) until the exit sub-pupil (position  $\rho'_i$ ) is  $\theta \cdot \rho_i$  (entrance OPD due to the source off-axis) minus  $\alpha \cdot \rho'_i$  (exit OPD due to the array reconfiguration), with  $\alpha$  the angle position considered on the image plane. If the array reconfiguration is an homothetic remapping such as  $\rho'_i = \gamma_b \rho_i$ , a central peak is formed on the detector at the angular position  $\theta/\gamma_b$ . The instrumental OPD is assumed to be null (*i.e.* the interferometer is cophased on-axis).

(the normalization factor has been eliminated for readability):

$$I(\alpha) \approx A(\alpha) \cdot O(\gamma_b \alpha) \otimes I_0(\alpha). \quad (10)$$

A convolution relationship between the object and the image remains inside the envelope, provided that the beam combiner keeps the pattern of the sub-aperture centers unchanged. This condition is less restrictive than the original formulation of the golden rule (Traub 1986) claiming that a strict homothetic mapping, including the sub-pupils (*i.e.* the Fizeau scheme), was required. This rule is true only if an infinite DIF is required. But, as we have demonstrated in section 2.1, an infinite DIF is useless for a diluted interferometer since the exploitable field is limited by the incomplete coverage of the  $(u, v)$  plane.

If an homothetic reconfiguration of the array preserves the convolution relation over a finite FOV, a non-homothetic one completely destroys it. Such a remapping however may be useful to make the sparse interferometric pupil suitable for coronagraphy. In this particular case, a second remapping restores the geometry of the array, after the coronagraph, to recover the convolution relationship (Guyon & Roddier 2002).

Equation 10 has been deduced using the hypothesis of a quite wide, immobile envelope position: the following sub-

sections detail what happens to the envelope with real combiners.

### 3.2 Fizeau combination

The first all-to-one beam combination scheme proposed for direct imaging was a strict homothetic mapping scheme, also called Fizeau, where the output pupil (seen from the focal plane) is a reduced copy of the entrance pupil (seen from the sky).

For the Fizeau scheme, the homothety ratio of the baselines  $\gamma_b$  is compensated by an identical homothety of the sub-apertures  $\gamma_d = d'/d$ , where  $d$  and  $d'$  represent the diameter of a sub-aperture in the entrance and in the output pupil plane respectively (Fig. 5). In this way, envelope  $A$  becomes the diffraction lobe of an aperture of diameter  $\gamma_d d$ , referred to as  $A_{\gamma_d d}$ . The beam compression increases the slope of the wavefront of each beam by the factor  $1/\gamma_d$ , therefore shifting the envelope to the angular position  $\theta/\gamma_d$  (with  $\theta$  the source off-axis). Equation 7 can now be rewritten as:

$$I(\alpha, \theta) = A_{\gamma_d d} \left( \alpha - \frac{\theta}{\gamma_d} \right) \times \left| \sum_{i=1}^{n_T} \exp \frac{-2i\pi}{\lambda} \left( \alpha - \frac{\theta}{\gamma_b} \right) \cdot \rho'_i \right|^2. \quad (11)$$

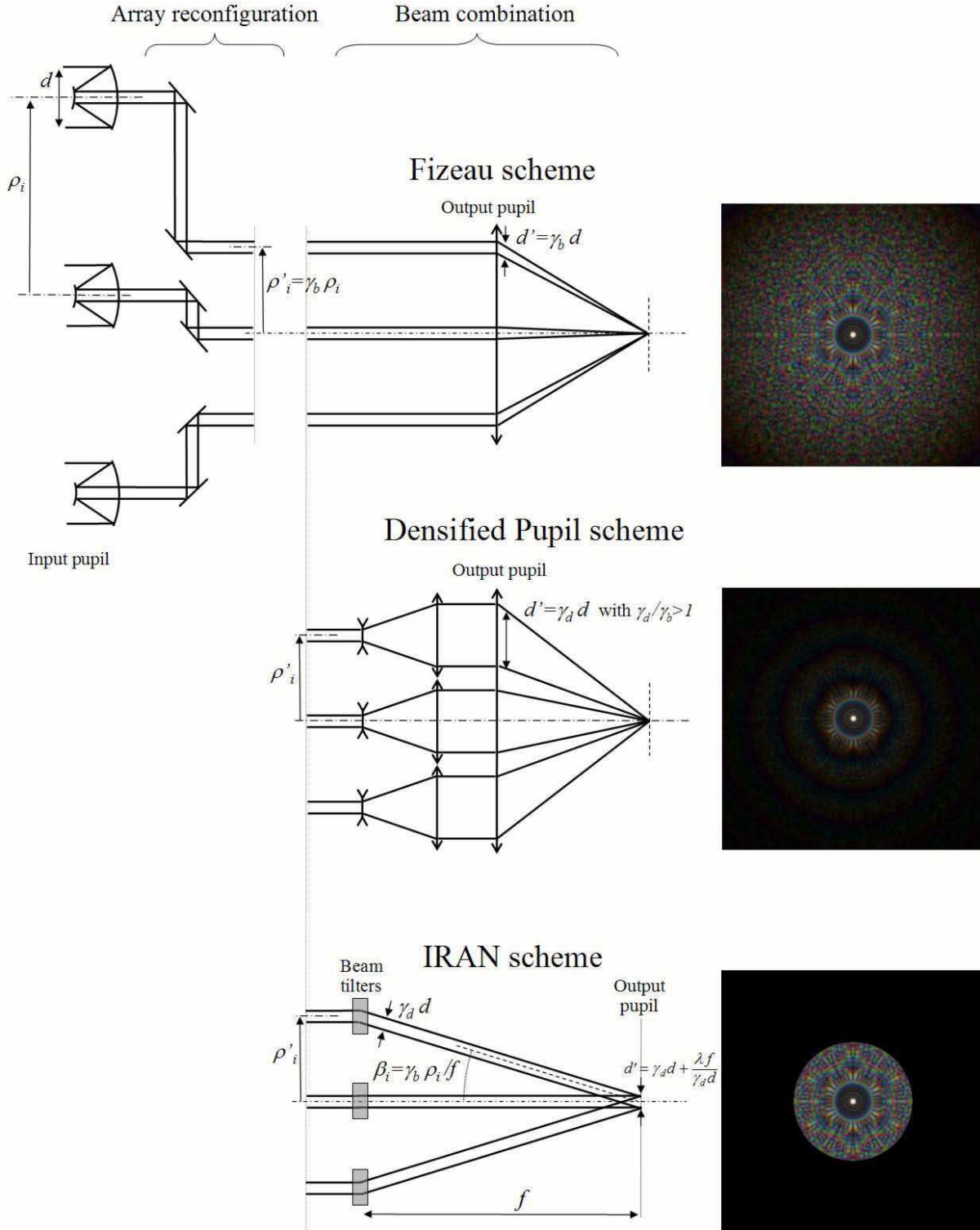


**Figure 5.** The three beam combination schemes considered for direct imaging (Fizeau, Densified Pupil and IRAN) and their corresponding PSF for a KEOPS-like array. A very generic version of IRAN, called IRAN<sup>b</sup> by Aristidi et al. (2004), is represented here. A previous version, called IRAN<sup>a</sup> (Vakili et al. 2004b), forms an intermediate image plane. Both versions of IRAN are strictly equivalent and are described by the same formalism. The Fizeau PSF spreads in numerous dispersed sidelobes over  $\lambda/d$ , while the Densified Pupil and the IRAN schemes can concentrate more flux inside the usable clean field (CLF) thanks to a narrower envelope (an Airy-shaped envelope and a flat top-hat envelope respectively). Relay lenses forming the output pupil have been omitted for clarity, and the beam diffraction is ignored for the IRAN PSF calculation (polychromatic PSF:  $\Delta\lambda/\lambda = 0.2$ , intensity scale in power 0.3).

Since  $\gamma_d = \gamma_b$ , interference pattern and envelope are translated of the same amount ( $\theta/\gamma_b$ ): the Fizeau PSF is translation invariant (Fig. 6) and the image of an extended source can be rigorously written as a convolution product:

$$I(\alpha) = O(\gamma_b \alpha) \otimes [A_{\gamma_b d}(\alpha) \cdot I_0(\alpha)]. \quad (12)$$

### 3.3 Densified Pupil combination

The technique of pupil densification was introduced (Labeyrie 1996) to provide more luminous images than in the Fizeau case: it concentrates the extremely wide and dispersed Fizeau PSF into the central interference peak (Fig. 5). The sparse aperture of an interferometer is now compatible even with coronagraphy (Labeyrie 1996; Guyon & Roddier 2002; Riaud et al. 2002). Thanks to pupil densification, the interferometer can work very much like any conventional telescope. This distinctive use of an interferometer has been called “hypertelescope”.

According to Labeyrie, a hypertelescope is a multi-aperture interferometer where the detecting camera is illuminated through an exit pupil which is a densified copy of the entrance aperture. “Densified copy” implies that the pattern of exit pupil centers is conserved with respect to the entrance pattern, while the size of the elementary sub-pupils is magnified, for example by an inverted Galilean telescope (Fig. 5). The densification is quantified by a dimensionless, convention-independent coefficient  $\gamma = \gamma_d/\gamma_b$ . This technique is a simple 2-D generalization of Michelson’s original truss (Michelson & Pease 1921).

When the pupil is densified, equation 11 remains valid but this time,  $\gamma_d/\gamma_b > 1$ . For an off-axis source (position  $\theta$ ), the fringe pattern is shifted to the angular position  $\theta/\gamma_b$ , while the envelope is shifted to a lower angular position:  $\theta/\gamma_d$  (Fig. 6). There is therefore no more strict object-image convolution relationship and equation 9 has to be updated. The densified pupil image is given by:

$$I(\alpha) = \iint O(\theta) A_{\gamma_d d} \left( \alpha - \frac{\theta}{\gamma_d} \right) I_0 \left( \alpha - \frac{\theta}{\gamma_b} \right) d^2 \theta. \quad (13)$$

For highly diluted arrays, the pupil densification can be so strong (*i.e.*  $\gamma_d/\gamma_b \gg 1$ ) that the shift of the envelope becomes negligible in comparison with the shift of the fringe pattern. We therefore meet the conditions of validity of the general equation 10, and can apply here the same steps used from Equ. 9 to Equ. 10:

$$I(\alpha) \approx A_{\gamma_d d}(\alpha) \cdot O(\gamma_b \alpha) \otimes I_0(\alpha). \quad (14)$$

A convolution relation remains, but in a FOV limited by the envelope of a densified sub-aperture only.

### 3.4 IRAN combination

The Interferometric Remapping Array Nulling (hereafter IRAN) beam combination scheme was introduced by Vakili et al. (2004b), and proposed for the already mentioned KEOPS project. IRAN was proposed as an alternative to the hypertelescope reconfiguration to prevent the loss of classical object-image convolution relation that it suffers during the pupil remapping. The solution proposed by the authors consists in recording the interference in a pupil plane rather than in the image plane (Fig. 5).

This solution exhibits appealing features for direct imaging, compared to the pupil densification. The moving Airy-shaped envelope of the hypertelescope is indeed replaced by a flat top-hat envelope, whose position is independent of the position of the sources. Thanks to this unique property, the formalism of image formation in the pupil-plane is simplified (Equ. 15) and the PSF becomes translation-invariant inside the top-hat.

The IRAN combiner performs again a non purely homothetic remapping of the wavefront, characterized by the two magnification coefficients  $\gamma_d$  and  $\gamma_b$  introduced in the previous section. Because the IRAN scheme preserves the geometry of the array, the interference function is unchanged. The image can be expressed exactly as a convolution product from equation 10:

$$I(\alpha) = P_{d'}(\alpha) \cdot O(\gamma_b \alpha) \otimes I_0(\alpha), \quad (15)$$

with  $P_{d'}$  a top-hat shaped envelope of diameter  $d'$ , whose position is independent from the source off-axis (Fig. 6), as in the case of a strong pupil densification. To be rigorous, the diffraction of the output collimated beams have to be considered, especially if output pupil size  $d'$  becomes comparable to the diffraction lobe (Sec. 4.2.2). In this case, the function  $P_{d'}$  is more exactly a top-hat function convolved with an Airy function. The total width of  $P_{d'}$  becomes:

$$d' = \gamma_d d + \frac{\lambda f}{\gamma_d d}. \quad (16)$$

Then, the IRAN envelope is actually flat only in the central part (the geometrical diameter of the output pupil) and features diffracted edges (the second term of the sum).

### 3.5 Single-mode fiber combination

Compared to classical bulk optics, single-mode fibers offer a very convenient solution for the beam transportation from the telescope focus towards the combiner (Lai et al. 2003). They apply also a spatial filtering which could improve the performances drastically in presence of residual phase errors (Coude Du Foresto, Ridgway, & Mariotti 1997). This spatial filtering induces no information loss with highly diluted interferometers, since we are only interested in the high spatial frequencies measured by the baselines, and not in low spatial frequencies measured by one sub-aperture.

Fibers are also of interest in direct imaging for the beam remapping and densification. Such a combiner has been proposed for a densified pupil imager on the VLTI (Lardi  re et al. 2004) and a demonstrator is under development in laboratory (Patru et al. 2006b).

As the tilt is lost in a single-mode fiber, the fringe envelope remains on-axis whatever the combination scheme and the densification factors. Then, the perfect convolution relationship provided by the Fizeau mode is destroyed by fibers. However, the Densified Pupil or the IRAN scheme can be used indifferently for combining the beams at the fiber outputs, the difference being only in the envelope shape. The fibred versions of both combination schemes are illustrated and studied in details by Patru et al. (2006a). In this paper, we will focus our attention on the envelope whose width determines directly the DIF.

The amplitude distribution of the output beam is a gaussian law, generally truncated by a collimating lens of

diameter  $d'$  and focal length  $f'$ . We refer to this distribution as  $\psi_{d',f'}(\mathbf{x})$ . Although the notion of pupil vanishes with fibers,  $d'$  defines a new output pupil diameter, and  $\gamma_d$  can again be defined as the ratio  $d'/d$ .

### 3.5.1 Fibred Densified Pupil scheme

As the Densified Pupil scheme forms the fringes in an image plane, the intensity distribution of the image is:

$$I(\boldsymbol{\alpha}) = |\text{FT}(\psi_{d',f'}(\mathbf{x}))|^2 \times I_0(\boldsymbol{\alpha} - \boldsymbol{\theta}/\gamma_b), \quad (17)$$

where FT denotes a Fourier Transform and  $I_0$  is the interference function defined in equation 8. Thus, the envelope becomes  $|\text{FT}(\psi_{d',f'}(\mathbf{x}))|^2$  and is not a pure Airy function as with classical optics (sec. 3.3) but a gaussian lobe convolved with an Airy lobe. As the envelope remains on-axis, we meet the exact conditions of validity of the general equation 10. Then, from equation 17, we can write the image of an extended object  $O$  as a convolution relationship:

$$I(\boldsymbol{\alpha}) = |\text{FT}(\psi_{d',f'}(\mathbf{x}))|^2 \cdot O(\gamma_b \boldsymbol{\alpha}) \otimes I_0(\boldsymbol{\alpha}). \quad (18)$$

Because the output beams have a gaussian profile, a full pupil densification is impossible. Then, there is a trade-off between the sensitivity gain provided by the densification and the flux lost by the beam truncation. Patru et al. (2006a) report that the maximum intensity is reached for  $d' = 2.2\omega(f')$ , with  $\omega(f')$  the radius where the amplitude is  $1/e$  times the maximum amplitude.

### 3.5.2 Fibred IRAN scheme

The IRAN scheme can also be used for combining beams behind single-mode fibers (Patru et al. 2006a). If the diffraction is negligible, the intensity distribution of the image is:

$$I(\boldsymbol{\alpha}) = |\psi_{d',f'}(\mathbf{x})|^2 \times I_0(\boldsymbol{\alpha} - \boldsymbol{\theta}/\gamma_b), \quad (19)$$

meaning that the envelope is directly the truncated gaussian profile and not its Fourier Transform as for the Densified Pupil case. Once again, as the envelope position is independent from  $\boldsymbol{\theta}$ , we can write the image of an extended object  $O$  as a convolution product:

$$I(\boldsymbol{\alpha}) = |\psi_{d',f'}(\mathbf{x})|^2 \cdot O(\gamma_b \boldsymbol{\alpha}) \otimes I_0(\boldsymbol{\alpha}). \quad (20)$$

As the maximum of the function  $|\psi_{d',f'}(\mathbf{x})|^2$  is always 1 whatever  $d'$ , the beam truncation has no effect on the central peak intensity and reduces the field only by vignetting.

## 4 FOV COMPARISON AND OPTIMIZATION

The previous section has shown that the choice of the beam combination scheme does not affect the interference function  $I_0$  if the array pattern is unchanged. The beam combiner simply applies, in a way, a “windowing” on this function, concentrating more flux on the central part of  $I_0$ . The width of this “windowing” defines the DIF. This section will compare the DIF of each beam combiner and will demonstrate that the Densified Pupil and the IRAN schemes can be optimized in order to match the DIF to the useful FOV, provided by the  $(u,v)$  plane coverage, *i.e.* the CLF.

## 4.1 DIF comparison

### 4.1.1 The Fizeau DIF

In a Fizeau scheme, an interferometer works strictly like a giant masked telescope magnifying the object  $1/\gamma_b$  times and preserving the convolution relationship between the object and the image over an infinite FOV (Equ. 12). The practical limits of the DIF are then imposed only by geometrical aberrations, vignetting or by the size of the detector. This advantage will be discussed in section 5.

### 4.1.2 The Densified Pupil DIF

Unlike the Fizeau case, the interference function is now modulated by an envelope of small diameter, which drastically reduces the DIF (Equ. 14). A non resolved off-axis source (position  $\boldsymbol{\theta}_0$ ) can *a priori* be correctly imaged as long as its central interference peak remains within the envelope (inside the FWHM by convention), *i.e.* :

$$\frac{\boldsymbol{\theta}_0}{\gamma_b} - \frac{\boldsymbol{\theta}_0}{\gamma_d} \leq \frac{\lambda}{2\gamma_d d}, \quad (21)$$

which constraints the diameter of the DIF, in radians on the sky:

$$\text{DIF}_\phi \approx \frac{\lambda}{(\gamma_d/\gamma_b - 1) d}. \quad (22)$$

For the fibred version of the Densified Pupil scheme, the envelope remains on-axis (Equ. 18). Then the DIF directly corresponds to the width of the envelope  $|\text{FT}(\psi_{d',f'}(\mathbf{x}))|^2$  (the FWHM by convention). For the optimal gaussian beam truncation, we find:

$$\text{DIF}_\phi \approx 1.13 \frac{\gamma_b}{\gamma_d} \cdot \frac{\lambda}{d}. \quad (23)$$

### 4.1.3 The IRAN DIF

The DIF of the IRAN scheme corresponds to the sky angular extent imaged over the output beams diameter  $d'$ . Considering that  $\gamma_b$  is the angular scaling factor from the sky to the detector and that the angular size of the output pupil, seen from the beam filters, is  $d'/f$  (Fig. 5), the DIF size on the sky can be written in radians from equation 16 as:

$$\text{DIF}_\phi = \frac{\gamma_b \gamma_d d}{f} + \frac{\gamma_b \lambda}{\gamma_d d}. \quad (24)$$

For the fibred version of the IRAN scheme, the output beam extent is now limited by the diameter of the collimating lens or by the detector size. If the output beam diameter is written  $\gamma_d d$ , then equation 24 remains valid for the fiber case.

## 4.2 Optimization of the DIF

The reduction of the DIF due to the pupil densification, compared to the Fizeau, is not at all a drawback as one could believe at first sight. The densification coefficients  $\gamma_b$  and  $\gamma_d$  are free parameters that can be used to concentrate more flux inside the field of interest. For instance, the densification can be adjusted to match the DIF to the CLF in order to maximize the luminosity gain. An analogue FOV optimization can *a priori* be found for the IRAN scheme.

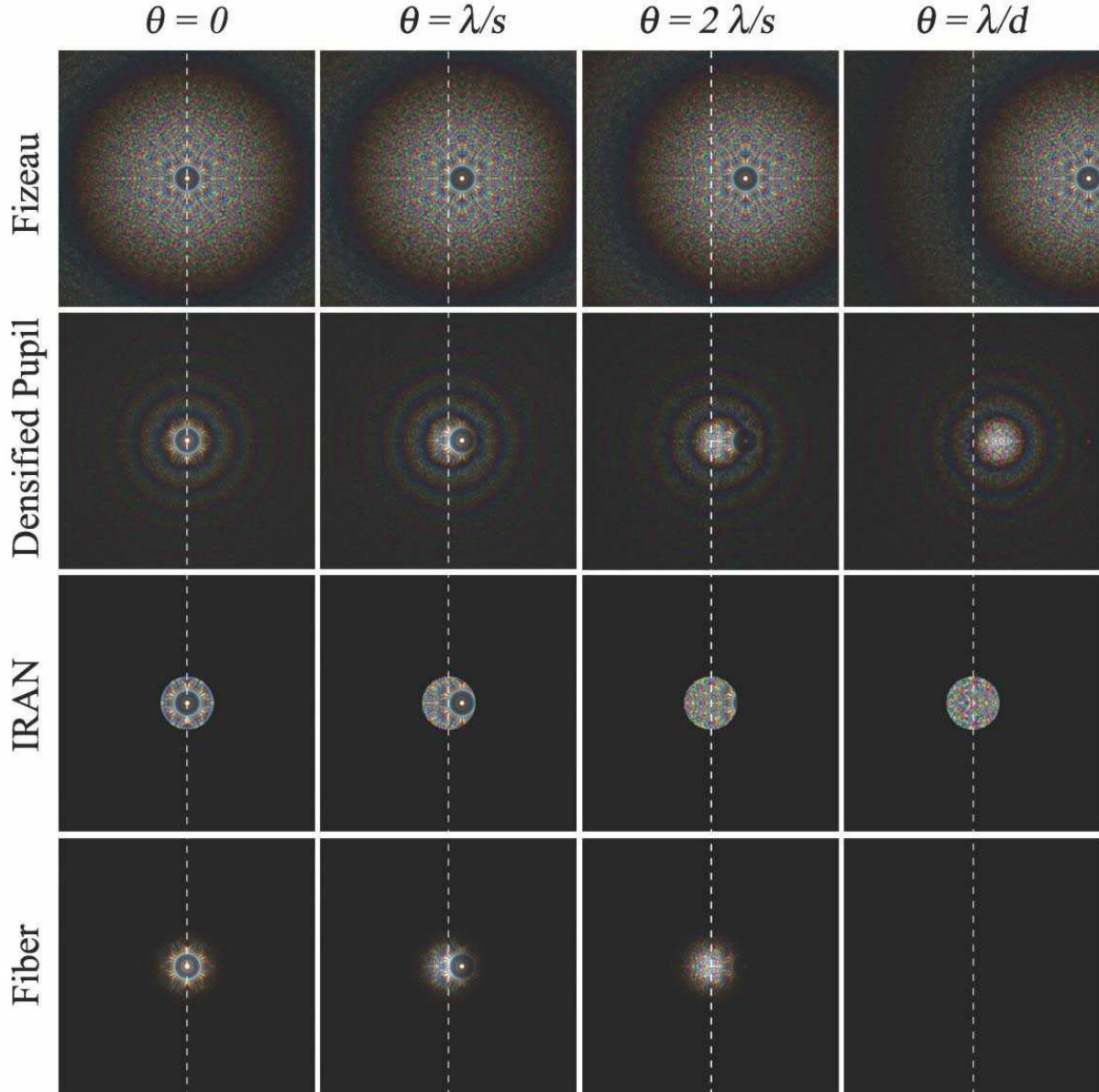


**Figure 6.** Fizeau PSF for different source off-axis, compared to PSF provided by a Densified Pupil, an IRAN and a fibred combination scheme (partial densification: DIF =  $2\lambda/s$ ). The  $\theta = 0$  and  $\theta = \lambda/s$  columns show a source inside the DIF for all the schemes. The  $\theta = 2\lambda/s$  column illustrates a source outside the DIF for all the schemes, excepted for the Fizeau case. The last column shows a source at the edge of the coupled field (CF) for the Fizeau, Densified Pupil and fibred schemes, but inside the CF for the IRAN scheme (polychromatic PSF:  $\Delta\lambda/\lambda = 0.2$ , intensity scale in power 0.3, beam diffraction is ignored for IRAN).

#### 4.2.1 Densified Pupil scheme optimization

The optimal pupil densification factors can be found by equalizing the equations 5 and 22. Assuming  $\gamma_d \gg \gamma_b$ , the pupil densification factor have to meet the following condition:

$$\frac{\gamma_d}{\gamma_b} \approx \frac{s}{d}, \quad (25)$$

with  $s$  the smallest typical spacing between apertures, and  $d$  the aperture diameter. This optimum occurs when two adjacent apertures of the array have their output pupils in contact. Note that this pupil densification was precisely the one originally proposed by Labeyrie (1996), but without introducing FOV considerations.

#### 4.2.2 IRAN scheme optimization

As for the hypertelescope mode, we can determine the densification factors  $\gamma_d$  and  $\gamma_b$  equalizing the DIF on the CLF for the IRAN combination scheme. To keep the main advantage of the IRAN, which is the flatness of the envelope  $P_{d'}$ , we choose to equalize only the flat part of the DIF (the first term of equation 24) with the CLF. From equations 24 and 5, this implies:

$$\gamma_d \gamma_b = \frac{\lambda f}{s d}. \quad (26)$$

This equation highlights the fact that the optimum is reached only for one wavelength, except if at least one of

the densification factors ( $\gamma_b$  or  $\gamma_d$ ) is proportional to  $\lambda$ . This chromatic issue does not exist in the Densified Pupil case. Indeed, if  $\gamma_d$  and  $\gamma_b$  are achromatic, the width of the envelope  $P_{d'}$  is not purely proportional to  $\lambda$  (Equ. 16), and cannot exactly follow the natural chromaticity of the CLF extent ( $\lambda/s$ ).

By introducing  $s' = \gamma_b s$ , the distance separating two adjacent afocal beams after the array remapping, equation 26 becomes:

$$s' = \frac{\lambda}{\gamma_d d} f, \quad (27)$$

meaning that the output beams are only separated by a diffraction lobe. In case of the IRAN<sup>a</sup> scheme (*c.f.* caption of figure 5), this condition occurs when the center of a sub-image coincides with the first zero of the neighboring sub-image. In other words, the intermediate image plane has to be fully densified. This result reminds us of the analogy with the Densified Pupil scheme: there is only an exchange between the pupil and the image planes.

If classical bulk optics are used, the minimal practical value of  $s'$  is reached when the output afocal beams are in contact, *i.e.*  $s' = \gamma_d d$ . Then equation 27 gives a new condition for  $\gamma_b$  and  $\gamma_d$ :

$$\frac{\gamma_d}{\gamma_b} = \frac{s}{d}. \quad (28)$$

Thanks to equations 26 and 28 it is possible to find a unique solution for both densification factors:

$$\gamma_b = \frac{\sqrt{\lambda f}}{s}, \quad \gamma_d = \frac{\sqrt{\lambda f}}{d}. \quad (29)$$

With these values, the central flat part of the DIF is equal to the diffractive part (Equ. 24). Then the total DIF is twice wider than the CLF (*i.e.*  $2\lambda/s$ ).

### 4.3 Luminosity gains

#### 4.3.1 Densified Pupil luminosity gain

The reason to be of pupil densification is to concentrate useless sidelobes flux in the central peak in order to provide much more luminous images than what the Fizeau allows. Actually, the pupil densification shrinks the carrier envelope  $A$  by a factor  $\gamma_d/\gamma_b$  in comparison to the Fizeau mode. Because the energy is conserved, the image is much brighter than in the Fizeau case, the gain being:

$$G = \left( \frac{\gamma_d}{\gamma_b} \right)^2. \quad (30)$$

In the optimized case, where the DIF and the CLF coincide, the intensity gain reaches its maximum. From equations 25 and 30, the best possible sensitivity gain is :

$$G_0 = \left( \frac{s}{d} \right)^2. \quad (31)$$

If single-mode fibers are used, the luminosity gain remains unchanged because the envelope width is almost unchanged. The only significant difference compared to bulk optics is the flux loss induced by the beam injection into the fiber (22% in the best case) and by the output beam truncation (8% in the optimized case (Patru et al. 2006a)).

#### 4.3.2 The IRAN luminosity gain

No considerations about the sensitivity were made by the authors of the IRAN scheme and yet, IRAN also can bring a valuable gain in luminosity compared to the Fizeau mode. Indeed, there is an intensification of the central peak if the support  $P_{d'}$  of the fringe pattern is narrower than  $\lambda/d$ , the *equivalent width* of the Fizeau envelope. From equation 24, the intensity gain provided by the IRAN scheme compared to the Fizeau is:

$$G = \left( \frac{\gamma_d}{\gamma_b} \cdot \frac{\lambda f}{\gamma_d^2 d^2 + \lambda f} \right)^2. \quad (32)$$

The best possible intensity gain, keeping the advantage of IRAN (the flat envelope), is reached when the flat part of the DIF coincides with the CLF. Its value is deduced from equations 29 and 32:

$$G_0 \approx \left( \frac{s}{2d} \right)^2, \quad (33)$$

that is 4 times lower than the optimal Densified Pupil case (Equ. 31).

### 4.4 Coupled FOV (CF)

#### 4.4.1 Definition

A beam combiner does not differ from others only in its DIF extent, but also in its coupled FOV (CF) extent. By analogy with spatial filters and optical fibers, we say that a source is “coupled” to the interferometer (*i.e.* located inside the CF), if some of its photons appear on-axis in the detector plane.

The CF is an important parameter to take into consideration because it determines the ease with which the interferometer may reach the crowding limit (Sec. 2.1). Indeed, the image of an on-axis object is polluted by the sidelobes of all surrounding sources present in the CF.

#### 4.4.2 Coupled FOV comparison

By convention, we assume that a source belongs to the CF if the on-axis pixel is located within the envelope  $A$  of the source. For the Fizeau case, the CF extent is  $\lambda/d$ , *i.e.* the radius of the diffraction lobe of a sub-aperture (Fig. 6).

For the Densified Pupil case, the CF can be determined from equation 11. The edge of the envelope  $A_{\gamma_d d}$  coincides with the central pixel when the source angular separation  $\theta_0$  meets the condition:

$$\frac{\theta_0}{\gamma_d} = \frac{\lambda}{\gamma_d d}. \quad (34)$$

Then, the CF is not dependent on the pupil densification factor and it is equal to  $\lambda/d$ , exactly as in the Fizeau case: the shrinking of the envelope is indeed compensated by the slower shift of the envelope (Fig. 6).

For IRAN, the fringe pattern is recorded in a pupil plane. The corresponding CF is therefore infinite by definition (Fig. 6), and the crowding becomes a serious issue. The use of a spatial filtering (pinhole or single mode fiber in each sub-image plane) can overcome this limit, but such a spatial filtering smoothes the output pupil edges. If a hole picks up only  $\lambda/d$  in each beam, the envelope  $P_{d'}$  becomes

	DIF	CF
Fizeau	$\infty$	$\lambda/d$
Densified Pupil	$\frac{\lambda}{(\gamma_d/\gamma_b - 1)d}$	$\lambda/d$
IRAN	$\gamma_b \gamma_d d/f$	$\infty$
Fibred DP	$\gamma_b/\gamma_d \cdot \lambda/d$	$\lambda/d$
Fibred IRAN	$\gamma_b \gamma_d d/f$	$\lambda/d$

**Table 1.** Direct Imaging Field (DIF) and Coupled Field (CF) of different combination schemes (in radians on the sky). The Fizeau DIF and the IRAN CF may formally be infinite, but some practical constraints, such as geometrical aberrations, vignetting or detector size, will limit these fields.

an Airy function exactly as for the Fizeau or the Densified Pupil schemes, and IRAN loses its main advantage.

Lastly, if single-mode fibers are used for the beam combination, the CF is obviously limited to  $\lambda/d$  (Fig. 6) whatever the chosen scheme (Densified Pupil or IRAN).

## 5 DISCUSSIONS

### 5.1 Identification of different FOV limitations

The keystone of this discussion about direct imaging with an interferometer is definitely the notion of field of view. It is a delicate notion that requires the introduction of four possible limitations:

- the information FOV (IF), which is the maximum angular size that a compact source can have without exceeding the crowding limit,
- the clean FOV (CLF), which corresponds to the useful clean central part of the PSF,
- the direct imaging FOV (DIF), inside which a source can be directly imaged by the interferometer, and
- the coupled FOV (CF), inside which any source spreads photons on the detector (for better or for worse).

The IF and the CLF are defined by the array configuration (respectively by the number of unique baselines and by the smallest typical baseline), while the DIF and the CF are imposed by the beam combination scheme. In addition to these four different fields, we can mention the existence of a fifth one: the “astrometric” FOV, over which high resolution measurements of angular separations are possible. As this field is generally not contiguous, we choose not to talk about wide field interferometry, contrarily to some authors (Montilla, Pereira, & Braat 2005) and refer to it as multi-field observation mode since it is an extension of the dual-field mode using differential delay-lines.

### 5.2 Choice of the beam combination scheme

Despite the unique characteristic of an infinite DIF, the use of a Fizeau combiner for highly diluted apertures appears excluded, because of PSF quality considerations. Indeed, the Fizeau PSF spreads in numerous secondary spectrally

dispersed peaks or speckles over a wide area (the diffraction lobe of a sub-aperture), which makes it poorly suited to high dynamic-range imaging (Fig. 5 and 6). This is the reason that motivated the development of other beam combiners such as the Densified Pupil and IRAN.

Moreover, a large DIF does not mean that any extended sources can be imaged properly. Section 2 has proved that the ultimate wide field imaging capabilities of an interferometer are already limited by the aperture array configuration (hence by the  $(u, v)$  plane coverage). Indeed, the finite number of apertures limits the maximum quantity of information recordable in a snapshot, while the shortest baseline  $s$  determines the angular size of the usable clean field (CLF).

Despite these considerations, the Fizeau scheme remains of interest for observing in a multi-field mode. The Fizeau focus acts as a natural spatial filter, which means that two sources separated by more than  $\lambda/d$  (the CF) can be observed simultaneously without interacting with each other. Such an observing mode preserves astrometric precision and involves neither star separators nor extra differential delay lines, contrarily to conventional dual field mode imaging.

A very attractive configuration therefore is to put an array of pupil densifiers and/or IRAN modules after the Fizeau focus. Such multi-field scheme benefits from both techniques. The Fizeau provides a wide FOV but unusable images, while the pupil densifiers focus on smaller fractions of the field and provide simultaneous directly exploitable images, as proposed in Labeyrie (2003). With this combination, all high angular resolution techniques used with conventional telescopes can be employed: speckle imaging with partial AO corrections or long exposure imaging, image deconvolution, etc. Each densifier may also include a coronagraph which opens the doors to high dynamic imaging with an interferometer.

The discussion is now about the choice between the Densified Pupil and the IRAN scheme. Our comparative study reveals that both combination schemes are fundamentally similar, the only difference being an exchange between the pupil and the image planes. This difference vanishes if single-mode fibers are used in either scheme, since the envelope has nearly the same shape and always remains on-axis (*c.f.* fig. 6 and table 1).

Both schemes can be optimized to equalize the DIF with the FOV delivered by the  $(u, v)$  plane coverage. This field optimization also induces an advantageous luminosity gain compared to the Fizeau mode, which can rise up to  $10^4$  for kilometric arrays (Eq. 31 and 33). In the optimized configuration, the hypertelescope mode features a fully densified output pupil, while IRAN features a fully densified intermediate image plane.

The classical bulk optics version of IRAN is unique because it offers a flat DIF, a particularity which can make the image deconvolution easier (Aristidi et al. 2004). However, its infinite CF makes IRAN not compatible for observing very extended sources or rich fields. Moreover, the IRAN scheme cannot concentrate the flux as efficiently as the hypertelescope does, because of the diffraction of the output beams. Indeed, equations 31 and 33 show that the luminosity gain is 4 times lower than the optimal Densified Pupil case. To reach the same gain, the size of the IRAN DIF should be decreased by a factor 2, meaning that the geometrical diam-

eter of the output pupil should be equal to zero in order to keep only the diffractive part. This implies that the fringes should be formed in an image plane rather than in a pupil plane, exactly as the Densified Pupil scheme does.

Therefore, the argument of an enhanced FOV for the IRAN scheme in comparison with the hypertelescope mode, initially invoked by Vakili et al. (2004b), should be moderated. The previous sections have already shown that the array itself induces a limit to the FOV which, anyway, cannot be overcome by the beam combiner.

## 6 CONCLUSION

The formal analysis introduced here demonstrates that the direct imaging capabilities of a diluted interferometer, *i.e.* the crowding limit, the PSF quality and the clean FOV, are determined by the choice of the geometry of the array only, and not by the choice of the beam combination scheme. This choice must be motivated by the science cases which will impose the necessary number of telescopes and decide to emphasize either FOV or dynamic range.

Among the available beam combination schemes for direct imaging, Densified Pupil and IRAN have been proven equivalent, except for a pupil-image plane inversion that changes the shape of a modulating envelope. The possibility to densify the array actually provides an optimal image reconstruction technique that fully exploits the field limited by the  $(u, v)$  plane coverage. It drastically improves the poor quality of the Fizeau PSF by concentrating the flux on a clean field of view only, while preserving all high angular resolution information.

Other aspects concerning the direct imaging, such as chromatic effects of beam combiners, array optimization and coronagraphy, will be studied in following papers. This study should provide sufficient matter to define the concept and the instrumentation of a future direct imaging large array, according to the top-level requirements (angular and spectral resolutions, FOV, dynamic-range, bandwidth, etc.) and the primary scientific goals.

## ACKNOWLEDGMENTS

The authors are very grateful to Denis Mourard and Antoine Labeyrie for fruitful discussions and also to Chris Haniff, the referee, for his comments on the manuscript.

## REFERENCES

Aime C., Soummer R., 2003, EAS, 8, 353

Aristidi E., Vakili F., Abe L., Belu A., Lopez B., Lanteri H., Schutz A., Menut J.-L., 2004, SPIE, 5491, 763

Baldwin J. E., Haniff C. A., Mackay C. D., Warner P. J., 1986, Nature, 320, 595

Coude Du Foresto V., Ridgway S., Mariotti J.-M., 1997, A&AS, 121, 379

Gillet S., et al., 2003, A&A, 400, 393

Gitti, M. Feretti, L. & Schindler, S., 2006, A&A, 448, 853

Goodman, J. W. 1996, "Introduction to Fourier Optics", Mc Graw Hill International Eds.

Guyon O., Roddier F., 2002, A&A, 391, 379

Hinz P. M., Connors T., McMahon T., Cheng A., Peng C. Y., Hoffmann W., McCarthy D. J., Angel R., 2004, SPIE, 5491, 787

Koechlin L., 2003, EAS, 8, 349

Koechlin L. & Perez J. P., 2003, SPIE, 4838, 411

Labeyrie A., Koechlin L., Lemaitre G., 1986, SPIE, 628, 323

Labeyrie A., 1996, A&AS, 118, 517

Labeyrie A., 2003, EAS, 8, 327

Lai O., et al., 2003, SPIE, 4838, 1296

Lardi  re O., Mourard D., Patru F., Carbillot M., 2004, SPIE, 5491, 415

Le Coroller H., Dejonghe J., Arpesella C., Vernet D., Labeyrie A., 2004, A&A, 426, 721

Michelson A. A., Pease F. G., 1921, ApJ, 53, 249

Montilla I., Pereira S. F., Braat J. J. M., 2005, ApOpt, 44, 328

Patru F., Mourard D., Lardi  re O., 2006, to be published

Patru F., et al., 2006, SPIE, 6228, to be published

Pedretti E., Labeyrie A., Arnold L., Thureau N., Lardi  re O., Boccaletti A., Riaud P., 2000, A&AS, 147, 285

Quirrenbach A., 2004, SPIE, 5382, 214

Riaud P., et al., 2002, A&A, 396, 345

Rottgering H., Jaffe W. J., Meisenheimer K., Sol H., Leinert C., Richichi A., Wittkowski M., 2004, SPIE, 5491, 9

Soummer R., Aime C. & Falloon P. E., 2002, A&A, 397, 1161

Traub W. A., 1986, ApOpt, 25, 528

Tuthill, P. G., Monnier, J. D. & Danchi, W. C., Nature, 398, 487

Vakili F., et al., 2004, SPIE, 5491, 1580

Vakili F., Aristidi E., Abe L., Lopez B., 2004, A&A, 421, 147